This paper is published as part of a *Dalton Transactions* theme issue on:

Nanomaterials for alternative energy sources

Guest editor: Andrew Barron
Rice University, Houston, Texas, USA

Published in issue 40, 2008 of *Dalton Transactions*

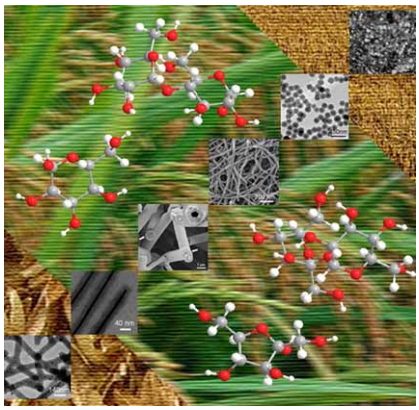

Image reproduced by permission of Shu-Hong Yu

Other papers published in this issue include:

Nanostructured thin solid oxide fuel cells with high power density
Alex Ignatiev, Xin Chen, Naijuan Wu, Zigui Lu and Laverne Smith, *Dalton Trans.,* 2008, DOI: 10.1039/b805658g

Inorganic nanomaterials for batteries
M. Stanley Whittingham, *Dalton Trans.,* 2008, DOI: 10.1039/b806372a

Raman spectroscopy of charge transfer interactions between single wall carbon nanotubes and [FeFe] hydrogenase
Jeffrey L. Blackburn, Drazenka Svedruzic, Timothy J. McDonald, Yong-Hyun Kim, Paul W. King and Michael J. Heben, *Dalton Trans.,* 2008, DOI: 10.1039/b806379f

Shape control of inorganic materials *via* electrodeposition
Kyoung-Shin Choi, *Dalton Trans.*, 2008, DOI: 10.1039/b807848c

Visit the *Dalton Transactions* website for more cutting-edge inorganic materials research
www.rsc.org/dalton

Raman spectroscopy of charge transfer interactions between single wall carbon nanotubes and [FeFe] hydrogenase

Jeffrey L. Blackburn,* Drazenka Svedruzic, Timothy J. McDonald, Yong-Hyun Kim, Paul W. King and Michael J. Heben

Received 15th April 2008, Accepted 3rd June 2008
First published as an Advance Article on the web 24th July 2008
DOI: 10.1039/b806379f

We report a Raman spectroscopy study of charge transfer interactions in complexes formed by single-walled carbon nanotubes (SWNTs) and [FeFe] hydrogenase I (CaHydI) from *Clostridium acetobutylicum.* The choice of Raman excitation wavelength and sample preparation conditions allows differences to be observed for complexes involving metallic (m) and semiconducting (s) species. Adsorbed CaHydI can reversibly inject electronic charge into the LUMOs of s-SWNTs, while charge can be injected and removed from m-SWNTs at lower potentials just above the Fermi energy. Time-dependent enzymatic assays demonstrated that the reduced and oxidized forms of CaHydI are deactivated by oxygen, but at rates that varied by an order of magnitude. The time evolution of the oxidative decay of the CaHydI activity reveals different time constants when complexed with m-SWNTs and s-SWNTs. The correlation of enzymatic assays with time-dependent Raman spectroscopy provides a novel method by which the charge transfer interactions may be investigated in the various SWNT–CaHydI complexes. Surprisingly, an oxidized form of CaHydI is apparently more resistant to oxygen deactivation when complexed to m-SWNTs rather than s-SWNTs.

Introduction

One way to build a sustainable energy economy is to use solar energy to split water. The energy stored can then be accessed by reacting hydrogen with oxygen to generate power in a fuel cell or internal combustion engine. Since the waste product of the reaction is only water, the cycle is completely closed and generates no greenhouse gases. With this future in mind, low cost materials are being sought for efficient solar-to-hydrogen and hydrogen-to-electricity conversion technologies. Currently, the scale-up of such devices is limited by a reliance on catalysts derived from expensive precious metals, such as platinum. Ideally, one inexpensive catalyst made from abundant materials could be used for both hydrogen production and oxidation, which would reduce costs, streamline manufacturing, and facilitate large-scale development.

Fortunately, a variety of microorganisms biosynthesize hydrogenases, a group of metalloenzymes that catalyze the hydrogen half-reaction ($2H^+ + 2e^- \leftrightarrows H_2$).[1] Hydrogenases are biocatalysts involving only a polypeptide chain and abundant first-row transition metals, and can potentially be incorporated into electrochemical cells[2,3] or molecular devices[4] as cheap, renewable, and efficient alternatives to noble metal catalysts. However, a number of technical hurdles limit the effectiveness of hydrogenases in biomimetic systems. Irreversible inhibition of some hydrogenases by oxidation represents one such challenge. Another major challenge is to achieve a robust and efficient electronic interaction between hydrogenase and other non-biological system components in a manner that does not compromise enzymatic activity.

National Renewable Energy Laboratory, Material Science, 16253 Denver West Parkway, Golden, Colorado, 80401, USA

Single-wall carbon nanotubes (SWNTs) are interesting candidates for use as molecular wires within bio-hybrid systems because of their nanoscale dimensions (comparable to the dimensions of a protein), high surface area, and outstanding electrical conductivity. Several recent reports in the literature have demonstrated that carbon nanotubes provide a useful scaffolding for electroactive enzymes, allowing for biological detection,[5–7] cellular delivery,[8,9] or improved immobilization on non-biological materials.[10] More recently, two reports have shown that considerably improved electron transfer efficiency between hydrogenase and an electrode surface can be achieved by utilizing carbon nanotubes.[11,12]

Recently, we demonstrated that the [FeFe] hydrogenase CaHydI from *Clostridium acetobutylicum* spontaneously forms stable, catalytic, complexes with semiconducting SWNTs (s-SWNTs) in solution.[13] Formation of the complexes, denoted as [SWNT|CaHydI], sensitized the s-SWNTs to the proton-H_2 redox couple through the catalytic activity of CaHydI. We followed photoluminescence (PL) emission quenching and studied electron transfer into the LUMO of the s-SWNTs. The PL quenching depended on the relative position of the SWNT LUMOs and the redox potential of the hydrogen half reaction, the latter of which was tuned by changing the H_2 partial pressure above the solution.

As-produced SWNT samples consist of both semiconducting and metallic species in a ratio of ~2 : 1. Consequently, we assumed that the metallic (m) SWNTs present in our samples also formed complexes with CaHydI. However, the existence or behavior of possible [m-SWNT|CaHydI] complexes could not be determined by PL spectroscopy because of the finite density of states between the HOMO and LUMO levels in m-SWNTs which prevent band-edge PL. Raman spectroscopy offers a powerful complement to PL spectroscopy as it enables studies of charge transfer interactions with both s- and m-SWNTs.[14,15] Vibrations specific to m- and

s-SWNTs can be determined through the judicious selection of Raman excitation wavelength (λ_{ex}).[16] Moreover, charge transfer can significantly affect the intensity, position, and shape of the SWNT Raman peaks by modifying the resonance conditions and/or altering the electron density between C–C bonds. We find Raman spectroscopy to be an ideal compliment to PL in the study of the [SWNT | CaHydI] complexes because it permits analysis of non-emissive m-SWNTs while also providing additional information on [s-SWNT | CaHydI] complexes.

In this report, we present a comprehensive Raman investigation of HipCO SWNTs complexed with CaHydI. We observed that the Raman signals associated with the radial breathing modes (RBMs) and tangential (G) modes are significantly modified for both s- and m-SWNTs and describe these observations in terms of charge transfer processes mediated by adsorbed CaHydI. Selection of λ_{ex} allows the charge transfer reactions with s- and m-SWNTs to be followed independently, and fast acquisition times permit the kinetics of the interactions to be assessed. In agreement with our PL results,[17] the Raman data confirm that s-SWNTs accept electrons from the reduced form of the enzyme ($CaHydI_{red}$) into the s-SWNT LUMO. Static and dynamic Raman spectra demonstrate that m-SWNTs accept electrons from both the reduced ($CaHydI_{red}$) and oxidized ($CaHydI_{ox}$) forms of the enzyme. The results suggest that an oxidized form of $CaHydI_{ox}$, which is generated by complexation with m-SWNTs, is more stable towards oxygen deactivation than is free $CaHydI_{ox}$. Oxygen deactivation assays on the free enzyme suggest that a key factor for oxygen sensitivity is protection of the distal, catalytic iron site from oxygen attack. The results from this study may be helpful for designing catalytic SWNT | CaHydI bio-hybrids, and may also suggest potential pathways to increase the oxygen tolerance of highly oxygen-sensitive bio-catalysts.

Experimental

As produced HipCO SWNTs were purchased from Carbon Nanotechnologies Incorporated (CNI) (Lot R0576, quoted purity >65 wt%) and were used without any further purification. Aqueous SWNT dispersions were produced by ultrasonication of SWNT powders in 1% (mg ml^{-1}) solutions of sodium cholate (SC), followed by centrifugation with a swing bucket (SW28) rotor at 28000 rev min^{-1} (141 000 *g*) for 4 h.[18] Sonication was performed with a Cole Palmer 750 W 1/4″ ultra-sonic tip at 40% power for 40 min, while the sample was cooled by 20 °C water flowing in an external jacket. Dispersions were investigated in 1 cm cuvettes.

The [FeFe] hydrogenase from the bacterium *Clostridium acetobutylicum* (CaHydI) was overexpressed in *E. coli* and purified as described previously.[19] The concentration of purified CaHydI in stock solutions varied between 1–2 mg ml^{-1}, and the specific activity varied between 200–400 U mg^{-1} (1 U is equivalent to 1 μmol H_2 produced per minute). Specific activity was determined by measuring the rate of H_2 evolution by gas chromatography in the presence of 25 mM methyl viologen after the enzyme was reduced by an excess of sodium dithionite in a 100 mM TES buffer (pH 7). Similar techniques were used to compare the rates at which molecular oxygen irreversibly deactivated neat CaHydI and CaHydI complexed with SWNTs. For these experiments, solution aliquots were taken as a function of time, immediately mixed with 25 mM sodium dithionite in 100 mM TES buffer (pH 7), and purged with Ar for 5 min to remove any traces of O_2 or H_2 prior to measuring the rate of H_2 evolution. Hydrogen evolution was initiated by addition of reduced methyl viologen.

To produce [SWNT | CaHydI] bio-hybrids, stock solutions of SWNT and CaHydI were first diluted with 100 mM TES buffer (pH 7), equilibrated with either a 4% H_2 (in N_2) or pure Ar atmosphere, and than simply mixed together and incubated at least one hour prior to measurements. CaHydI was diluted 20 fold in the preparation of final solutions from the stock. Catalytic activity of CaHydI was stable in the presence of SWNTs for at least several weeks.[17] The final concentrations of sodium cholate were diluted to be ≤0.3 wt% (3 mg ml^{-1}) to avoid denaturation of the CaHydI.

We measured the properties of [SWNT | CaHydI] bio-hybrids prepared by four different procedures. The preparations were chosen in an effort to poise CaHydI at intermediate states in the catalytic cycle. Previous spectroscopic and spectroelectrochemical studies have shown that similar [FeFe] hydrogenases from *Clostridium pasteurianum* can be poised by employing redox or H_2/pH controlled conditions.[20] By analogy, we expect similar behavior for CaHydI. Fig. 1 shows cartoon representations of the four different preparations. Preparation **1** was the control sample, which contained only SC-dispersed SWNTs, with no enzyme added. In the absence of enzyme, SWNTs were insensitive to the gaseous environment (H_2, Ar, or air), so **1** was conveniently investigated in lab air. In preparation **2**, the SWNT and CaHydI solutions were equilibrated under 4% H_2 and then mixed to create the bio-hybrid. In this case, we expect the enzyme solution to be comprised of predominantly the reduced form of the enzyme ($CaHydI_{red}$), with the oxidized enzyme ($CaHydI_{ox}$) being the minority species. Preparation **3** resulted when **2** was purged with Ar for 45 min. Here we expect the enzyme's redox state to be shifted further towards the oxidized but catalytically active form, $CaHydI_{ox}$, and the partial pressure of H_2 is estimated be ~10^{-7} atm following our previous work.[17] In preparation **4** the headspace of the enzyme and SWNT solutions were purged with Ar for 8 h prior to mixing. In this case, we expect $CaHydI_{ox}$ to be the dominant enzyme species in solution prior to mixing.

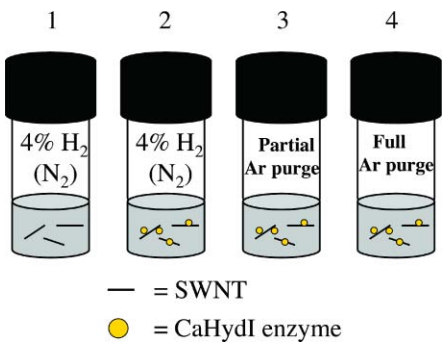

Fig. 1 Cartoon exhibiting four different conditions under which [SWNT | CaHydI] bio-hybrid samples were prepared and examined. Preparation **1**, the control sample, consists of HipCO SWNTs dispersed in 0.3% sodium cholate in H_2O under a headspace gas of 4% H_2 in N_2. Preparation **2** was obtained by combining **1** with a CaHydI-containing solution while reducing conditions (4% H_2) were maintained. Preparation **3** is **2** purged with Ar for ~45 min. Condition **4** is a [SWNT | CaHydI] mixture prepared from individual samples that had been purged under Ar for 8 h prior to mixing.

Raman spectra were recorded in a backscattering configuration, with excitation at 532 nm from a frequency-doubled YAG laser, or 632.8 nm from a Helium/Neon (HeNe) laser.[21] Time dependent measurements were performed without changing the position of the cuvette, and no flocculation was observed during these experiments. Laser output was monitored during measurement to ensure a constant excitation power for each spectrum. Photoluminescence spectra were obtained in a front-face configuration in a modified Fourier transform instrument with excitation from a tungsten lamp coupled to a monochromator.[22] Theoretical calculations of SWNT electronic structure were calculated as previously described.[23–26]

Results and discussion

Static solution-phase Raman spectroscopy experiments were first performed to analyze the electronic interactions in [SWNT|CaHydI] complexes formed in the various equilibrated preparations. Fig. 2a shows data taken with 633 nm excitation in the RBM region for the control sample (preparation **1**), a mixture of SWNTs and CaHydI that was prepared under 4% H_2 (preparation **2**), and a mixture of CaHydI and SWNTs which was extensively purged under Ar before mixing (preparation **1**). The RBM signals are in the range of ~180 to 300 cm^{-1}, as expected for the typical HipCO diameter distribution (~0.8–1.2 nm). Note that this choice of excitation wavelength allows for the behavior of s- and m-SWNTs to be discerned: peaks below 225 cm^{-1} correspond to excitation of the larger diameter m-SWNTs *via* the first metallic resonance (M_{11}), while the peaks above 225 cm^{-1} are associated with smaller diameter s-SWNTs excited *via* the second excitonic transition (S_{22}). Comparing the data from **2** and **1**, a dramatically reduced intensity RBM intensity is observed for s- and m-SWNTs after CaHydI is complexed under the reducing conditions. As discussed in detail below, these finding are explained by CaHydI-mediated electron injection, in agreement with our previous PL study on [s-SWNT|CaHydI] complexes. In contrast, data from **4** shows that the s-SWNT RBM modes are unaffected relative to **1**, while the m-SWNT modes were significantly attenuated. In this case, the data suggest that electron injection occurs to a significant extent only for the m-SWNTs, while charge injection does not occur appreciably for s-SWNTs. It is important to note that the spectra can be normalized to one another by obtaining additional Raman data after the preparations were equilibrated with lab air, as shown in the next section. This procedure completely deactivates the enzyme, returns all SWNTs to their intrinsic electronic state in solution, and permits differences in concentration to be directly assessed since the spectra are virtually identical except for a scaling factor, thus enabling normalization.

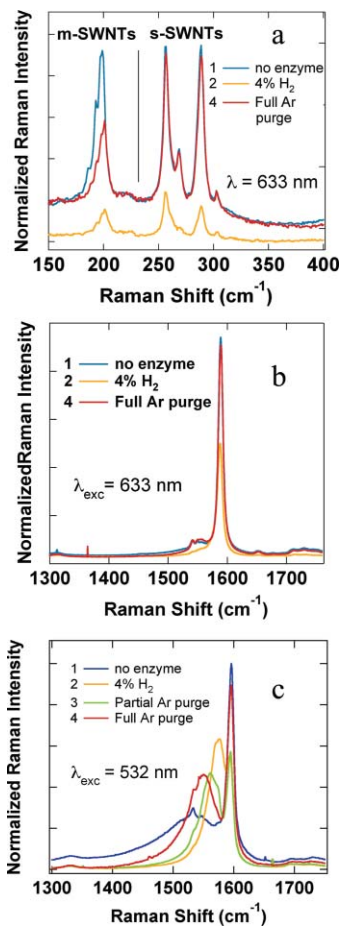

Fig. 2 Raman spectra of SWNT in various preparations at equilibrium. (a) RBM region at $\lambda_{ex} = 633$ nm. (b) G-Band region at $\lambda_{ex} = 633$ nm. (c) G-Band regions at $\lambda_{ex} = 532$ nm.

Fig. 2b shows the G band spectra for the same samples excited at 633 nm. Due to the particular resonance conditions for the m-SWNTs and s-SWNTs with 633 nm light, the G^+ mode is dominated by s-SWNTs, and overshadows the broad metallic G^- mode. Thus, in contrast to the RBM data, the m-SWNT behavior is not as clearly discerned in the G-band region of the spectrum with $\lambda_{ex} = 633$ nm (Fig. 2b). Data from **1** shows a dominant, sharp G^+ mode at 1592 cm^{-1} from s-SWNTs and a small G^- shoulder at ~1530 cm^{-1} from m-SWNTs.[16] In **2**, the intensity of the G^+ mode is reduced by ~50%, while the m-SWNT G^- mode is much less intense, slightly narrower, and blue-shifted. The sample purged with Ar before mixing (**4**) showed a semiconducting G^+ peak with the same intensity as **1**, while the metallic G^- mode was slightly narrower and blue-shifted relative to **1**.

The G-band spectra change dramatically when $\lambda_{ex} = 532$ nm (Fig. 2c). At this wavelength, s-SWNTs are excited resonantly *via* the third (S_{33}) excitonic transition, and similar intensities are observed for both the G^+ and G^- modes. As a result, the extreme sensitivity of the G^- mode to the preparation conditions becomes readily apparent. In **1**, the G^- is at 1528 cm^{-1} and has a width of ~80 cm^{-1}. In **2**, the G^- mode is significantly blue-shifted to ~1580 cm^{-1} and strongly narrowed to ~20 cm^{-1}. When the headspace of **2** is purged with Ar for 45 min (preparation **3**), the G^- broadens (~35 cm^{-1}) and the peak position (1560 cm^{-1}) moves towards the value obtained for **1**. When samples were purged extensively prior to mixing (**4**), the G^- mode is at 1545 cm^{-1} with a width of ~50 cm^{-1} - close to, but still significantly different than the control sample (**1**). No new information is obtained regarding the semiconducting G^+ mode with $\lambda_{ex} = 532$ nm: the G^+ mode in **2** and **3** is attenuated by nearly 50% relative to **1**, while the G^+ mode is barely affected under preparation **4**, in complete agreement with observations made with $\lambda_{ex} = 633$ nm (Fig. 2b).

Summarizing the findings for s-SWNTs presented in Fig. 2, the G^+ and RBMs are significantly attenuated under the more reducing conditions with H_2 present (preparation **2**), and a slight

increase in intensity is observed for these modes when the H_2 partial pressure is reduced in the headspace by purging with Ar (preparation **3**). An interpretation based on electron injection into s-SWNT LUMOs under **2** and removal under **3** is consistent with the changes observed for s-SWNT PL under identical experimental conditions.[17] In that case, the PL of all s-SWNTs was quenched under 4% H_2 due to electron injection mediated by CaHydI when the potential of the H^+/H_2 half reaction was poised at approximately –0.37 V *vs.* NHE. Electron occupation of the s-SWNT LUMO quenches the PL and diminishes the resonance Raman conditions for s-SWNTs, which attenuates the intensity of both tangential and radial vibrational modes. When the headspace was purged with Ar (preparation **3**), PL from a few of the smallest diameter SWNTs became observable again due to a positive shift in the H^+/H_2 redox potential to approximately –0.20 V. Consistent with PL, the Raman intensity is restored as charge is withdrawn from the s-SWNTs and a new equilibrium is established. Smaller diameter tubes are not reversibly changed because their LUMO levels lie at more positive electrochemical potentials. The full PL intensities for all s-SWNT species are seen in the PLE map for condition **4** (not shown), suggesting that the H^+/H_2 redox potential lies below the LUMO of all s-SWNT species, preventing electron injection. Consistently, the RBM and G^+ modes in condition **4** are similar to the control sample. Fig. 3 shows the position of the LUMO level for the (6,5) species, which is one of the smallest diameter s-SWNTs in our sample, as well as the electrochemical potential of the hydrogen half reaction under preparations **2**, **3**, and **4**. The potential for condition **4** is only an estimate, based on the observation that PL from all s-SWNTs is seen under this condition. The alignment of the (6,5) LUMO with the different redox potentials makes it clear how changes in the H_2 partial pressure can lead to dramatic changes in both the PL and Raman data based on charge equilibration.

The responses of the m-SWNTs in the RBM region (Fig. 2a) are quite similar to that of the s-SWNTs, except for one important difference. As with the s-SWNTs, the m-SWNT RBM modes are strongly attenuated under condition **2** (4% H_2), but, in contrast, they remain reduced in intensity even after 8 h of Ar purging (**4**). Although it is clear that the redox potential of the hydrogen couple has been shifted to more oxidizing potentials under these conditions, it is difficult to indicate an exact potential for this preparation in Fig. 3. However, it is clear that the electronic properties of the m-SWNTs are significantly perturbed in condition **4**, suggesting that charge transfer has occurred under these conditions.

The effects on the m-SWNT G^- modes are more complex, and must be discussed in terms of the changing position, intensity, and width of this broad peak. The energy and width of the G^- mode depends on the Fermi energy of the metallic SWNTs, which determines the energy window for coupling of the G phonon to electronic excitations near the Dirac point.[27–29] Similar to the case of graphene,[30] the energy and width of the G^- mode have a minimum and maximum, respectively, when SWNTs are undoped and the Fermi energy is at the Dirac point. As the Fermi energy is moved away from the Dirac point to either higher or lower energy (n- or p-type doping), the G^- mode narrows and blue-shifts, providing a useful indicator of intentional or unintentional doping.[27,29] In the present case, the progressive red-shifting and broadening of the G^- mode seen in spectra **2**, **3**, and **4** suggests that the Fermi level is moved more positive toward the intrinsic case (**1**) as the ambient environment is made less reducing. These effects are displayed schematically in the *Ek* diagrams on the right side of Fig. 3. The top case depicts an n-doped m-SWNT and the bottom case depicts an intrinsic m-SWNT. For the intrinsic m-SWNT, the G^- electronic coupling to virtual e^-h^+ pairs (left side) and real e^-h^+ pairs (right side) gives rise to a large energetic dispersion that leads to a red-shifted and broad G^- peak. Phonon damping *via* decay into vertical e^-h^+ pairs (right side) controls the G^- peak width, while the creation and annihilation of virtual e^-h^+ pairs (left side) re-normalizes the phonon energy. After injection of electrons from CaHydI, the energetic dispersion of the phonon–electron coupling is diminished by the Pauli exclusion principle, leading to a narrowing of the G^- mode and re-normalization to higher energy.

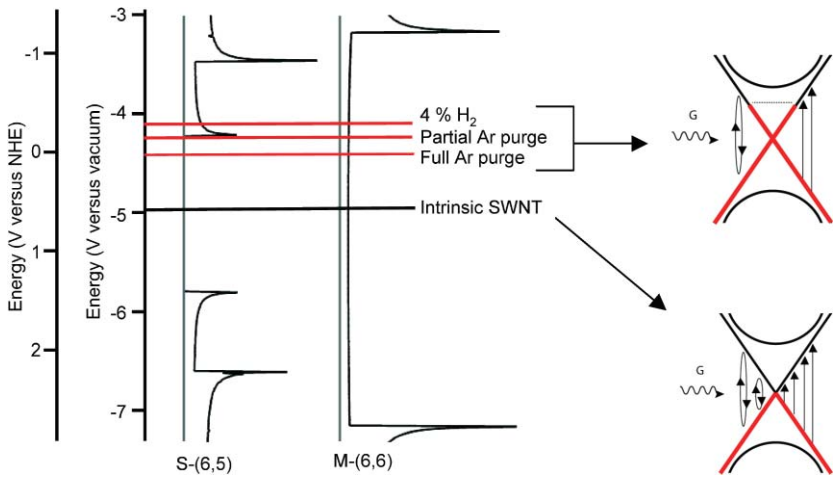

Fig. 3 Left: Calculated density of states for an (6,5) s-SWNT and an (6,6) m-SWNT are plotted *versus* energy on both an electrochemical scale, where the normal hydrogen electrode (NHE) is zero, and *versus* vacuum. Red lines show the approximate Fermi level for the various SWNT dispersions studied in this report, as confirmed by photoluminescence, absorbance, Raman spectroscopy, and the Nernst equation. Right: *Ek* diagrams showing how the G^- phonon of m-SWNTs is re-normalized and broadened by coupling to electronic excitations near the Dirac point.

The changes in the G^- mode are fully consistent with expectations based on electron injection. This arises from the fact that, in contrast to s-SWNTs that can only accept electron density into the LUMOs, unoccupied mid-gap states above the Fermi level in m-SWNTs can accept electrons at potentials below the first conduction band singularity. The observation that m-SWNTs are significantly affected by complexation under **4** is quite intriguing considering that the CaHydI is expected to be fully poised at $CaHydI_{ox}$. The data suggest that electron density can still be transferred from $CaHydI_{ox}$ to unoccupied states above the m-SWNT Fermi level. An alternative explanation based on electron withdrawal to render m-SWNTs p-type is unlikely based of the large positive potential that would be required (>+0.7 V *vs.* NHE).

Fig. 4a and 4b show Raman data for [SWNT | CaHydI] complexes equilibrated under preparation **2** and then exposed to lab air at $t = 0$. The experiments were designed to probe how the charge injected into SWNTs was affected when CaHydI complexed to SWNTs was deactivated by O_2. As before, we focus on G-band data taken with $\lambda_{ex} = 532$ nm and RBM data obtained with $\lambda_{ex} = 633$ nm to elucidate the behaviors of m- and s-SWNTs separately. Considering the G-band first (Fig. 4a), exposure to O_2 causes the initial G^+ intensity to increase and saturate at the intensity of **1** after ~29 min. In contrast, the G^- mode evolved much more slowly,

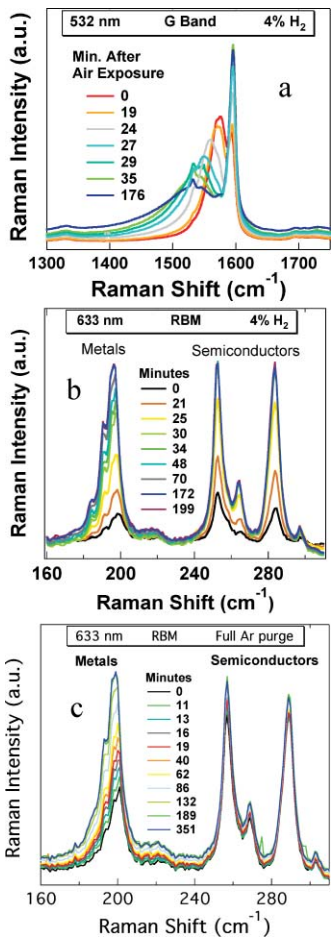

Fig. 4 Time-dependence of Raman spectra after preparations were exposed to air. (a) G-Band data taken at $\lambda_{ex} = 532$ nm for **2**, (b) RBM data taken at $\lambda_{ex} = 633$ nm for **2**, and (c) RBM data taken at $\lambda_{ex} = 633$ nm for **4**.

broadening and red-shifting such that its shape eventually returned to that seen for **1** over the course of several hours. Fig. 4b shows the same basic result from the perspective of the RBM data. The attenuated RBM signals seen for **2** return to the values seen for **1** after exposure to O_2. Once again, the s-SWNT peaks saturate at the control sample (**1**) values after ~30 min, while the peaks for m-SWNTs require several hours to return completely to their unperturbed intensities. Both data sets show that the rate at which the m- and s-SWNTs return to their unperturbed states differs significantly, which indicates that the kinetics of O_2 deactivation depend on whether CaHydI is bound to m- or s-SWNT species.

For comparison, we examined the rate at which SWNTs in **4** relaxed upon exposure to air (Fig. 4c). In agreement with data in Fig. 2, the s-SWNT modes were not appreciably affected by complex formation under these conditions, so minimal change with exposure to air was expected or seen. Also in agreement with Fig. 2, the m-SWNT RBMs were initially attenuated, but not to the same degree seen for preparation **2**. Again, less electron injection is possible, and only into m-SWNTs, when complexes were formed under Ar. In this case, the m-SWNT RBM modes evolve back more slowly to their unperturbed intensities than when m-SWNTs were deactivated from preparation **2** (Fig. 4b). This is surprising since (*vide infra*) one expects $CaHydI_{red}$ to be more O_2 tolerant than $CaHydI_{ox}$ and, furthermore, it may be expected that the complexes formed under **2** should be stabilized against deactivation to some degree by the reducing equivalents initially present on the SWNTs.

A more quantitative assessment is gained by plotting the changes in the Raman signals shown in Fig. 4 as a function of time. Kinetics for m- or s-SWNTs can be obtained from the intensity of the G^- or G^+ mode, respectively, with $\lambda_{ex} = 532$ nm, or by integrating the area under the m- or s-SWNT RBMs when $\lambda_{ex} = 633$ nm. Fig. 5a displays the results of this analysis, with the data normalized to values of zero initially and unity when the Raman response had stopped changing. This presentation format makes it clear that for a given type of SWNT (m or s) the kinetics for restoration of the Raman signals to the unperturbed values seen for **1** are independent of whether the G-band or RBM responses are examined. Furthermore, it can be readily seen that the kinetics for deactivation are significantly different for s- and m-SWNTs, and that the kinetics of the latter are strongly dependent on the sample preparation conditions.

Table 1 displays the kinetic constants obtained by fitting exponential rise times to the data in Fig. 5a. All curves for s-SWNT kinetics could be fit to a single exponential time constant with values of ~$4–5 \times 10^{-3}$ s^{-1}. This rate is close to the values reported for the PL recovery from s-SWNTs which were studied under the same conditions ($2.5–4 \times 10^{-3}$ s^{-1}). Thus, it seems clear that the recovery of the Raman and PL signals has the same origin in the case of s-SWNTs. Specifically, electrons injected into the s-SWNT LUMOs, mediated by complexed CaHydI under reducing conditions, are removed as the enzyme is deactivated in O_2. In contrast, m-SWNT traces required two time constants to be fit, with one being similar in magnitude to the time constant for s-SWNTs, and a second that was an order of magnitude slower ($2–5 \times 10^{-4}$ s^{-1}, Table 1). Interestingly, the relative contribution of the slow time constant depended on the method under which the complex was prepared. For complexes prepared under 4% hydrogen (**2**), m-SWNT kinetics were dominated by the fast component (~90%), whereas the slow time constant dominated (90%) when samples were extensively

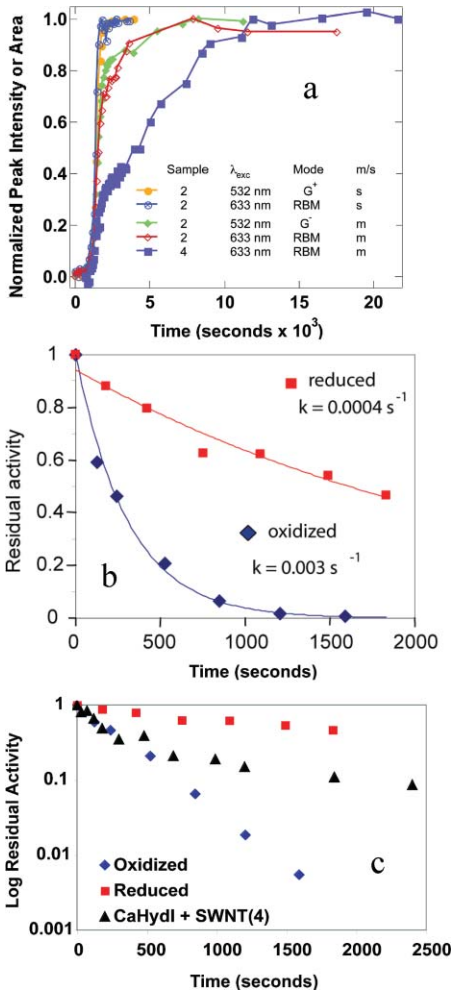

Fig. 5 (a) Kinetics of return of Raman signals after SWNT–enzyme complexes were exposed to air, utilizing either RBM or G-band data in Fig. 2 (see text). (b) Residual H_2-evolving activity of $CaHydI_{red}$ and $CaHydI_{ox}$ upon exposure to O_2 (see text). (c) Residual activities of the free CaHydI (from top) are compared with the residual activities of CaHydI mixed with SWNTs after extensive purging with Ar (condition **4**). Activity data are presented in logarithmic scale to better illustrate single *versus* bi-exponential functionality.

purged with Ar prior to mixing (**4**). The fast component is the same as that observed for the s-SWNT kinetics in reducing conditions, and the relative contribution of this component is consistent with what is qualitatively expected for the enzyme equilibrium from Le Chatelier's principle. In reducing conditions (4% H_2), $CaHydI_{red}$ dominates, and after purging with Ar, $CaHydI_{red}$ becomes the minority species. However, the existence of the slow time constant suggests that m-SWNTs may interact with $CaHydI_{ox}$ to produce a more oxygen-tolerant species.

In an effort to understand the origin of the different time constants observed for deactivation of the complexes we examined the rate of CaHydI deactivation in the absence of SWNTs (Fig. 5b). A solution containing primarily $CaHydI_{ox}$ was prepared by extensive Ar sparging[20] and the rate of deactivation upon exposure to air was measured by determining the enzyme's ability to continue to produce hydrogen (*vide supra*). In this case, the activity decay fit a single exponential function with a time constant of ~3×10^{-3} s^{-1}. Evaluating the rate at which $CaHydI_{red}$ was deactivated by O_2 was not as straightforward. To keep the enzyme poised in the reduced state, O_2 was injected into a capped vial containing 4% H_2 to achieve an O_2 concentration the same as air (21%). The head space composition was verified by gas chromatography, and aliquots were withdrawn periodically and analyzed for hydrogen evolution activity. The activity decay for $CaHydI_{red}$ also fit a single exponential function, but with a ten-fold lower time constant of ~4×10^{-4} s^{-1}.[31] Note that if $CaHydI_{red}$ prepared under 4% H_2 was simply exposed to air the activity decay was biexponential (data not shown), as expected for time constants corresponding to both the faster and slower rates observed for $CaHydI_{ox}$ and $CaHydI_{red}$, respectively. Thus, we found the rate of CaHydI deactivation by O_2 to be clearly dependent on the oxidation state of the enzyme. This can be qualitatively understood by considering that the distal Fe in CaHydI, the site at which both catalysis and, presumably, irreversible oxidation occurs, is more likely to be occupied by H_2 when in the reduced form, and therefore protected against reaction with O_2 to some degree.[32]

Interestingly, the assayed rate for $CaHydI_{ox}$ deactivation is the same as the single rate seen for the return of the s-SWNT Raman signals when **2** was exposed to air, which is the same as the dominant rate seen for m-SWNTs deactivation from **2** (Table 1). This is somewhat surprising considering that preparation **2** contains 4% H_2, which should poise the enzyme primarily in the $CaHydI_{red}$ state. Naively, one might expect SWNT deactivation from **2** to occur at the same rate seen for $CaHydI_{red}$ or, alternatively, at both a slow and a fast rate, as was observed when the activity of $CaHydI_{red}$ was assayed after opening the sample to air. Though our understanding is not complete, the findings suggest either a more efficient conversion of *bound* $CaHydI_{red}$ to $CaHydI_{ox}$, which might be a result of more efficient O_2 transport to the enzyme when complexed with SWNTs, or a change in oxidation state of

Table 1 Rate constants obtained from fits to kinetics of the Raman spectroscopy data for air-exposed [SWNT | CaHydI] complexes and free CaHydI. The preparations (prep) and analysis methods are described in the text. Metallic SWNTs required two time constants to fit the biexponential data, with the slower component, (k_2), dominating the response to differing degrees (%k_2)

Sample	Preparation	λ_{ex}/nm	m- or s-SWNT (mode)	k_1/s^{-1}	k_2/s^{-1}	%k_2
[SWNT | CaHydI]	**2**	633	s-SWNT (G^+)	0.0047	—	0
[SWNT | CaHydI]	**2**	633	s-SWNT (RBM)	0.0053	—	0
[SWNT | CaHydI]	**2**	633	m-SWNT (RBM)	0.0033	0.00047	10
[SWNT | CaHydI]	**2**	532	s-SWNT (G^+)	0.0042	—	0
[SWNT | CaHydI]	**2**	532	m-SWNT (G^-)	0.003	0.0002	11
[SWNT | CaHydI]	**4**	633	m-SWNT (RBM)	0.005	0.0002	90
CaHydI	**4**	—	—	0.003	—	0
CaHydI	**2**	—	—	—	0.0004	100

the enzyme due to the charge injection process itself. The former scenario could be the result of improved transport for O_2 in the gas channels due to conformational changes in the enzyme structure due to complexation. The latter scenario could result from direct electron transfer from $CaHydI_{red}$ to the SWNT, such that the bound enzyme, now in the $CaHydI_{ox}$ state, decayed with the rate of free $CaHydI_{ox}$. Clearly, these issues require further study.

Even more surprising is the fact that [m-SWNT|CaHydI] complexes exhibit two rate constants for deactivation *via* Raman spectroscopy, and that the slower rate ($\sim 2 \times 10^{-4}$ s^{-1}), the one similar to the rate of O_2 deactivation assayed for the H_2-poised enzyme (Table 1), is dominant when preparation **4** is exposed to air. This is surprising because $CaHydI_{ox}$ is expected to be the dominant species in **4**, and the rate for $CaHydI_{ox}$ deactivation assayed in SWNT-free solutions was fast (3×10^{-3} s^{-1}, Table 1). This could be rationalized if $CaHydI_{ox}$ were able to pull enough electronic charge from m-SWNTs under these relatively oxidizing conditions to become $CaHydI_{red}$. This would explain why the deactivation kinetics are comparable to those assayed for poised $CaHydI_{red}$. However, such a process would entail removing electrons from m-SWNTs, rendering them p-type, and is unlikely because of the large positive potential required, $>+0.7$ V *vs.* NHE, as discussed above.

A more palatable explanation can be constructed by considering the behavior of some other [FeFe] hydrogenases. For example, when *Desulfovibrio vulgaris* and *D. desulfuricans* are initially purified in the presence of O_2 they transition to an O_2 insensitive, non-catalytic state, $H_{ox}{}^{air}$.[1,33] This occurs *via* a 1 or 3 electron oxidation of the oxidized catalytic form of the enzyme, H_{ox}, through an intermediate state, H_{trans}.[34,35] Within this context, $CaHydI_{ox}$ might undergo oxidation by charge transfer to m-SWNTs under condition **4**. Both the electron density still present in $CaHydI_{ox}$ and the thermodynamics of the exchange suggest this is possible. As a result $CaHydI_{ox}$ would transition to a more oxidized H_{trans}-like state. This oxidized form of $CaHydI_{ox}$ might have a coordinatively saturated H-cluster due to formation of an exchangeable ligand, *e.g.* OH^-, at the active distal iron site and may therefore be less reactive to O_2. Following the idea that $CaHydI_{ox}$ is protected against O_2 deactivation only when complexed to m-SWNTs we performed an assay of the residual H_2 evolution activity after complexes prepared under **4** were exposed to lab air. Fig. 5c shows the data plotted with the residual activity for free $CaHydI_{ox}$ and $CaHydI_{red}$ (reproduced from Fig. 5b). Consistent with our view, both the fast and slow rates of deactivation are observed, and the transition from fast to slow occurs at ~70% residual activity. This corresponds to the expected ratio between semiconducting to metallic SWNTs (2 : 1), as expected if the surface density of CaHydI was equal on both m- and s-SWNTs and the enzyme bound to s-SWNTs was deactivated more quickly than the enzyme complexed to m-SWNTs.

Conclusion

In conclusion, we have performed a detailed solution-phase Raman study of charge transfer that occurs in complexes formed between SWNTs and the [FeFe] hydrogenase CaHydI. The analysis of Raman modes specific to either semiconducting or metallic SWNTs allows us to follow static or dynamic charge transfer events that have a critical dependence on the SWNT electronic structure. In agreement with our previous study, we find that s-SWNTs interact solely with the reduced enzyme, accepting electrons created by the oxidation of H_2. In contrast, the continuous density of states between the first van Hove singularities in m-SWNTs allows electron injection from both the reduced and oxidized forms of the enzyme. Our results suggest that purified m-SWNTs or s-SWNTs, rather than mixed preparations, may be more suitable in the fabrication of [SWNT|CaHydI] bio-hybrids for specific applications due to greater control of the bio-hybrid electronic properties. In particular, s-SWNTs might be better suited for use in solar-driven devices, in which the strongly absorbing, tunable HOMO–LUMO transitions could be used to couple energy into the [SWNT|CaHydI] complex. In contrast, the high dark conductivity and continuous mid-gap density of states in m-SWNTs might make them better suited for hydrogen production or conversion in electrochemical applications. The recent demonstration of highly efficient separation of SWNTs by electronic structure[36] implies that rationally tailored SWNT/hydrogenase bio-hybrids could provide abundant, inexpensive, and scalable material alternatives for an emerging hydrogen economy.

Acknowledgements

This work was supported by the U.S. Department of Energy, Office of Science, Office of Basic Energy Sciences, Division of Chemical Sciences, Geosciences, and Biosciences.

References

1 W. Lubitz, E. Reijerse and M. vanGastel, *Chem. Rev.*, 2007, **107**, 4331–4365.
2 M. Hambourger, M. Gervaldo, D. Svedruzic, P. W. King, D. Gust, M. Ghirardi, A. L. Moore and T. A. Moore, *J. Am. Chem. Soc.*, 2008.
3 K. A. Vincent, J. A. Cracknell, O. Lenz, I. Zebger, B. Friedrich and F. A. Armstrong, *Proc. Natl. Acad. Sci. USA*, 2005, **102**, 16951–16954.
4 M. J. Esswein and D. G. Nocera, *Chem. Rev.*, 2007, **107**, 4022–4047.
5 W. Joseph, *Electroanalysis*, 2005, **17**, 7–14.
6 S. N. Kim, J. F. Rusling and F. Papadimitrakopoulos, *Adv. Mater.*, 2007, **19**, 3214–3228.
7 P. W. Barone, S. Baik, D. A. Heller and M. S. Strano, *Nat. Mater.*, 2005, **4**, 86–92.
8 A. Bianco, K. Kostarelos, C. D. Partidos and M. Prato, *Chem. Commun.*, 2005, 571–577.
9 N. W. Shi Kam, M. O'Connell, J. A. Wisdom and H. Dai, *Proc. Natl. Acad. Sci. USA*, 2005, **102**, 11600–11605.
10 F. Patolsky, Y. Weizmann and I. Willner, *Angew. Chem., Int. Ed.*, 2004, **43**, 2113–2117.
11 M. A. Alonso-Lomillo, O. Rudiger, A. Maroto-Valiente, M. Velez, I. Rodriguez-Ramos, F. J. Munoz, V. M. Fernandez and A. L. DeLacey, *Nano Lett.*, 2007, **7**, 1603–1608.
12 A.-R. Liu, T. Wakayama, C. Nakamura, J. Miyake, N. A. Zorin and D.-J. Qian, *Electrochim. Acta*, 2007, **52**, 3222–3228.
13 T. J. McDonald, D. Svedruzik, Y.-H. Kim, J. L. Blackburn, S. B. Zhang, P. King and M. J. Heben, *Nano Lett.*, 2007, **7**, 3528–3534.
14 M. S. Strano, C. B. Huffman, C. M. Moore, M. J. O'Connell, E. H. Haroz, J. Hubbard, M. Miller, K. Rialon, C. Kittrell, S. Ramesh, R. H. Hauge and R. E. Smalley, *J. Phys. Chem. B*, 2003, **107**, 6979–6985.
15 V. Skakalova, A. B. Kaiser, U. Dettlaff-Weglikowska, K. Hrncarikova and S. Roth, *J. Phys. Chem. B*, 2005, **109**, 7174–7181.
16 M. S. Dresselhaus, G. Dresselhaus, R. Saito and A. Jorio, *Phys. Rep.*, 2005, **409**, 47–99.
17 T. J. McDonald, D. Svedruzic, Y.-H. Kim, J. L. Blackburn, S. B. Zhang, P. King and M. J. Heben, *Nano Lett.*, 2007, **7**, 3528–3534.
18 M. J. O'Connell, S. M. Bachilo, C. B. Huffman, C. M. Moore, M. S. Strano, E. H. Haroz, K. Rialon, P. J. Boul, W. H. Noon, C. Kittrell, J. P. Ma, R. H. Hauge, R. B. Weisman and R. E. Smalley, *Science*, 2002, **297**, 593–596.

19 P. W. King, M. C. Posewitz, M. L. Ghirardi and M. Seibert, *J. Bacteriol.*, 2006, **188**, 2163–2172.
20 A. T. Kowal, M. W. Adams and M. K. Johnson, *J. Biol. Chem.*, 1989, **264**, 4342–4348.
21 J. L. Blackburn, C. Engtrakul, T. J. McDonald, A. C. Dillon and M. J. Heben, *J. Phys. Chem. B*, 2006, **110**, 25551–25558.
22 T. J. McDonald, M. Jones, C. Engtrakul, R. J. Ellingson, G. Rumbles and M. J. Heben, *Rev. Sci. Instrum.*, 2006, **77**, 053104/053101–053104/053106.
23 We used VASP27 and SIESTA28 to calculate electronic structures of various single-wall carbon nanotubes within the local density approximation (LDA)29. For plane-wave VASP calculations, we used the kinetic energy cutoff of 400 eV. LDA and experimental energy gaps of seven semiconducting chiral nanotubes were compared with diameters ranging 7.6–10.5 Å.[13] LDA underestimates the real electronic gaps by about 60% on average. For electronic density of states (DOS) of individual single-wall nanotubes, we used SIESTA to get one-dimensional band structures with double-zeta-polarization (DZP) basis sets, and took DOSLDA(E) = $2\sum \mathrm{d}k/\mathrm{d}E$, where the factor of 2 is for spin degeneracy and the summation runs over all bands. The DOSLDA(E) was scaled down by multiplying 0.574 as the LDA energy is smaller by 1.74 times than experiment.
24 J. M. Soler, E. Artacho, J. D. Gale, A. Garcia, J. Junquera, P. Ordejon and D. Sanchez-Portal, *J. Phys.: Condens. Matter*, 2002, **14**, 2745–2779.
25 G. Kresse and J. Joubert, *Phys. Rev. B*, 1999, **59**, 1758–1775.
26 D. M. Ceperley and B. I. Alder, *Phys. Rev. Lett.*, 1980, **45**, 566–569.
27 J. L. Blackburn, T. J. McDonald, W. K. Metzger, C. Engtrakul, G. Rumbles and M. J. Heben, *Nano Lett.*, 2008, **8**, 1047–1054.
28 D. Abdula, K. T. Nguyen and M. Shim, *J. Phys. Chem. C*, 2007, **111**, 17755–17760.
29 J. C. Tsang, M. Freitag, V. Perebeinos, J. Liu and P. Avouris, *Nat. Nanotechnol.*, 2007, **2**, 725.
30 J. Yan, Y. Zhang, P. Kim and A. Pinczuk, *Phys. Rev. Lett.*, 2007, **98**, 166802.
31 In the latter experiment (4% H_2 atmosphere) oxygen was added in the closed vial in order to keep hydrogen in the head space, with final concentration of O_2 close to 21%. If the $CaHydI_{red}$ (under 4% H_2) was simply exposed to air the activity decays as biexponential function (data not shown) with the time constants corresponding to faster and slower rates observed for $CaHydI_{ox}$ and $CaHydI_{red}$ respectively. We think that by exposing sample to air, H_2 gas diffuses out and as a consequence some $CaIHyd_{red}$ molecules get oxidized before reacting with O_2, mimicking the conditions of Ar treated sample. In order to test if the slower rate of O_2-inactivation in the presence of 4% H_2 is due to competition of gas molecules for the same binding site on the enzyme, we ran an experiment with a different ratio of H_2/O_2 (1 : 1, 10% each gas). The rate of inactivation was the same order of magnitude (0.0007 s^{-1}; data not shown) as for the described 1 : 5 H_2/O_2 ratio, not ruling out but suggesting that hydrogen does not inhibit CaIHyd inactivation by O_2.
32 A. Silakov, E. J. Reijerse, S. P. J. Albracht, E. C. Hatchikian and W. Lubitz, *J. Am. Chem. Soc.*, 2007, **129**, 11447–11458.
33 M. W. W. Adams, *Biochim. Biophys. Acta*, 1990, **1020**, 115–145.
34 A. S. Pereira, P. Tavares, I. Moura, J. J. G. Moura and B. H. Huynh, *J. Am. Chem. Soc.*, 2001, **123**, 2771–2782.
35 W. Roseboom, A. L. De Lacey, V. M. Fernandez, E. C. Hatchikian and S. P. J. Albracht, *JBIC, J. Biol. Inorg. Chem.*, 2006, **11**, 102–118.
36 M. S. Arnold, A. A. Green, J. F. Hulvat, S. I. Stupp and M. C. Hersam, *Nat. Nanotechnol.*, 2006, **1**, 60–65.